On the homogeneity and interpretation of precipitable water time series derived from global GPS observations

Author(s):
Vey, S.; Dietrich, R.; Fritsche, M.; Rülke, A.; Steigenberger, Peter; Rothacher, Markus

Publication date:
2009-05-27

Permanent link:
https://doi.org/https://doi.org/10.3929/ethz-c-000020130

Originally published in:
Journal of Geophysical Research: Atmospheres 113, https://doi.org/10.1029/2008JD010415

On the homogeneity and interpretation of precipitable water time series derived from global GPS observations

S. Vey,[1] R. Dietrich,[1] M. Fritsche,[1] A. Rülke,[1] Peter Steigenberger,[2] and Markus Rothacher[3]

Received 14 May 2008; revised 23 September 2008; accepted 25 February 2009; published 20 May 2009.

[1] Observations of the Global Positioning System (GPS) were reanalyzed over the period from 1994 to 2004 in a joint project of the technical universities in Dresden and Munich. The estimated tropospheric parameters were converted into precipitable water (PW) using surface pressure observations from the World Meteorological Organization and atmospheric mean temperature fields from the European Centre for Medium-Range Weather Forecasts. For the first time a systematic study of the homogeneity of global GPS-derived precipitable water time series was carried out regarding the influence of changes in the GPS antennas and radomes as well as changes in the number of recorded observations. The focus of this study is on interannual changes in precipitable water. Over Europe, large parts of North America, and Iceland and in the region south of 30°S, these changes are very small. The range of the PW variations on interannual time scales is less than 2 mm in these areas. However, in the southeastern part of North America and north Australia, these anomalies in precipitable water show a range of up to 6 mm. In the tropics, PW anomalies with a range of up to 10 mm were found. GPS PW was compared with a modeled PW assuming water vapor saturation. This shows that GPS PW of stations located in the middle and high northern and southern latitudes is consistent with the temperature-related saturation values of water vapor. In the tropics and subtropics the annual temperature variations are low. In these regions the variations in the PW can be dominated by other factors, including water vapor transport. At seasonal time scales the water vapor transport can be associated with atmospheric circulation such as monsoonal flow.

Citation: Vey, S., R. Dietrich, M. Fritsche, A. Rülke, P. Steigenberger, and M. Rothacher (2009), On the homogeneity and interpretation of precipitable water time series derived from global GPS observations, *J. Geophys. Res.*, *114*, D10101, doi:10.1029/2008JD010415.

1. Introduction

[2] The atmospheric water vapor significantly influences many processes of the Earth's weather and climate. Water vapor is a major greenhouse gas controlling the heat budget of the Earth [*Philipona et al.*, 2005]. Global, long and accurate water vapor observations are indispensable for the understanding, modeling and prediction of global weather and climate processes. However, at present the spatial distribution and the temporal variations of the water vapor are insufficiently known. Many details on the reaction of the hydrological cycle to climate changes, the so-called water vapor feedback mechanism, are not yet understood. Some climate models predict a 3 times higher temperature increase under a doubling CO_2 concentration when considering the effect of water vapor feedback compared to calculations neglecting the influence of water vapor [*Schneider et al.*, 1999; *Hall and Manabe*, 1999; *Held and Soden*, 2000; *Soden et al.*, 2002]. The climate prognoses are based on numerous assumptions and they are affected by large uncertainties [*Folland et al.*, 2001; *Su et al.*, 2006].

[3] The longest records of atmospheric humidity originate from radiosondes. A network of radiosondes has observed water vapor since about 1940 continuously. Humidity observations from radiosondes have been used to study water vapor variability and trends [e.g., *Elliott and Gaffen*, 1991; *Zhai and Eskridge*, 1996; *Ross and Elliott*, 1996, 2001]. However, the water vapor time series are very inhomogeneous owing to changes in the used sensors, in the observation periods and in the analysis strategies [*Garand et al.*, 1992; *Zhai and Eskridge*, 1996]. Measurements with different sensors can exhibit differences in the

[1] Institut für Planetare Geodäsie, Technische Universität Dresden, Dresden, Germany.
[2] Institut für Astronomische und Physikalische Geodäsie, Technische Universität München, Munich, Germany.
[3] Institut für Geodäsie und Photogrammetrie, Eidgenössische Technische Hochschule Zürich, Zurich, Switzerland.

0148-0227/09/2008JD010415

relative humidity of up to 20%. The systematic error in the relative humidity is mainly influenced by the calibration procedure of the sensor which is performed before the start of the radiosondes [*Soden and Lanzante*, 1996]. The reliability of the humidity measurements strongly decreases at temperatures below −30°C [*Elliott and Gaffen*, 1991; *Ferrare et al.*, 1995; *Miloshevich et al.*, 2001]. Small and very high humidity also reduces the accuracy of the humidity observations [*Miloshevich et al.*, 2006].

[4] Over the last 15 years observations from the Global Positioning System (GPS) provide a large database for the weather-independent estimation of water vapor [e.g., *Bevis et al.*, 1992; *Rocken et al.*, 1995; *Duan et al.*, 1996; *Yunck et al.*, 2000; *Wickert et al.*, 2005]. A big advantage of GPS-derived water vapor compared to radiosonde measurements is the independence of GPS observations on any sensor calibrations. In 1994 a global network of about 50 continuously observing GPS stations was established by the International GNSS (Global Navigation Satellite System) Service (IGS) [*Beutler et al.*, 1999]. Today this network has grown to 414 stations worldwide; therefrom 370 stations are active.

[5] Atmospheric water vapor causes a propagation delay of the GPS signal as it travels from the GPS satellite to the receiver. The signal propagation delay due to the atmospheric constituents including water vapor is estimated as an additional parameter in the GPS data processing. According to *Bevis et al.* [1994], the estimated tropospheric parameter, also referred to as zenith tropospheric delay (ZTD), can be converted into precipitable water using surface pressure and temperature. Precipitable water (PW) is defined as the total water vapor contained in an air column from the Earth's surface to the top of the atmosphere. Other terms used in this context are integrated or total column water vapor. PW derived from ground-based GPS measurements agrees very well with the observations from other systems like radiosondes or water vapor radiometers [e.g., *Rocken et al.*, 1993; *Tregoning et al.*, 1998; *Hagemann et al.*, 2003; *Deblonde et al.*, 2005; *Wang et al.*, 2007].

[6] Precipitable water from GPS measurements has widely been used to improve the weather forecast in different countries [e.g., *Gutman and Benjamin*, 2001; *Gendt et al.*, 2004; *Vedel et al.*, 2004; *Bock et al.*, 2005; *Guerova et al.*, 2006]. First climate related investigations of GPS-derived PW were carried out by *Gardinarsky et al.* [2002] and *Elgered et al.* [2003] showing an increase in PW of 7 to 14% per decade over Scandinavia in the time period from 1993 to 2002. *Foster et al.* [2000] demonstrated the impact of El Niño on precipitable water vapor using the observations of two GPS stations in the tropical Pacific in the years 1997 and 1998. *Bock et al.* [2007] analyzed the PW over Africa and showed its relation with the monsoon.

[7] While several regional studies have been conducted using GPS-derived PW for climate studies, only few emphasis has been placed on the global scale. *Hagemann et al.* [2003] and *Deblonde et al.* [2005] used data from the IGS network in order to validate global numerical weather forecast models. But, their analyses cover only a few months. A recently published PW data set derived from GPS observations covering the time period from 1997 to 2004 is based on the combined tropospheric parameters of the IGS analysis centers [*Wang et al.*, 2007]. The IGS tropospheric product is derived from operational GPS solutions and is therefore influenced by software changes and modifications of the processing strategies. Especially changes in the mapping function or the elevation cutoff angle can cause significant jumps of several millimeters in the time series of the estimated tropospheric parameters [*Gendt*, 1998]. Therefore, the time series of the IGS combined tropospheric solution can't be considered as homogeneous and are not applicable to climate studies. The 5-min ZTD data set at IGS sites produced by the precise point positioning approach is more homogeneous and therefore better suited for future climate studies than the legacy 2-hourly combined tropospheric parameters (S. H. Byun et al., The new tropospheric product of the International GNSS Service, paper presented at 2005 ION GNSS Conference, Institute of Navigation, Long Beach, California, 2005). However at present the 5-min ZTD data are only available from October 2000 onward.

[8] The goal of this study is to retrieve homogeneous PW time series from global GPS observations covering one decade of time. For this purpose the GPS data analysis strategy and the applied models have to be kept unchanged for the whole processing period. This can only be realized by a reprocessing of the global GPS data starting at the observation level. The reprocessing strategy and the derivation of PW from GPS tropospheric parameters is described in section 2. Section 3 is dedicated to the accuracy and to detailed investigations of the homogeneity of the estimated PW time series. In section 4, we perform an analysis of the PW time series with special focus on interannual changes in the PW. The question, how precipitable water is influenced by temperature changes will also be addressed. Additionally, we investigate the relation between PW anomalies and the Southern Oscillation. A summary and conclusions are given in section 5.

2. Estimation of Precipitable Water From GPS

2.1. Data Processing

[9] In a joint project of the Deutsches GeoForschungsZentrum and the Technical Universities in Dresden and Munich data of nominal 195 GPS stations were reprocessed. The reprocessing of the global GPS network covers the period from the beginning of 1994 to the end of 2004 and was carried out with a modified version of the Bernese GPS Software 5.0 [*Dach et al.*, 2007]. Details on the reprocessing strategy and the applied models are described by *Steigenberger et al.* [2006]. Here only the most important differences between the reprocessing and operational processing strategies of the IGS analysis centers will be given. These are: (1) the application of the isobaric hydrostatic mapping function based on data of the numerical weather prediction model of the ECMWF [*Niell*, 2000; *Vey et al.*, 2006], (2) the use of absolute antenna phase center variations for GPS receivers and satellites [*Schmid et al.*, 2005] and (3) the consideration of higher-order ionospheric effects [*Fritsche et al.*, 2005]. Some further processing aspects are: the elevation cutoff angle was set to 3° and an elevation-dependent weighting was applied to the data. The ZTD parameters were estimated continuous piecewise-linear in 2-h intervals and tropospheric gradients in NS and EW direction were estimated in 24-h intervals. The reprocessing

of the global network with 20 Pentium IV computers equipped with 2.4 and 3 GHz processors required 3 months of pure computation time.

[10] The conversion of the tropospheric parameters derived during the GPS data analysis into PW was carried out according to *Bevis et al.* [1994]. In a first step, the zenith wet delay (*ZWD*) is derived, by subtracting the zenith hydrostatic delay (*ZHD*) from the estimated *ZTD* parameters,

$$ZWD = ZTD - ZHD. \tag{1}$$

The ZHD can be modeled with sufficient accuracy from the air pressure P_s at the GPS antenna height using the equation of *Saastamoinen* [1972],

$$ZHD = \left[(0.0022768 \pm 0.0000005)\frac{\mathrm{m}}{\mathrm{hPa}}\right]\frac{P_s}{f(\varphi, h)}, \tag{2}$$

with

$$f(\varphi, h) = 1 - 0.0026\cos 2\varphi - 0.00028\left[\frac{1}{\mathrm{km}}\right]h. \tag{3}$$

[11] The term $f(\varphi, h)$ accounts for the dependence of the gravity acceleration from the ellipsoidal latitude φ and the ellipsoidal height h of the GPS station. In a second step the ZWD is converted into the corresponding amount of water vapor with the help of a conversion factor Π.

$$PW = \Pi \cdot ZWD. \tag{4}$$

Π varies as function of the water vapor weighted mean temperature of the atmosphere T_m [*Bevis et al.*, 1994],

$$\Pi = \frac{10^6}{\rho_w R_v\left(\frac{k_3}{T_m} + k_2'\right)}, \tag{5}$$

with

$\rho_w = 999.97$ (kg m^{-3}) density of liquid water;
$R_v = 461.51$ (J K^{-1} kg^{-1}) specific gas constant of water vapor;
k'_2 and k_3 atmospheric refraction constants ($k'_2 = 22.1 \pm 2.2$ (K hPa^{-1}), $k_3 = 373900 \pm 1200$ (K^2 hPa^{-1})).

[12] T_m of the atmosphere is very well represented by the global reanalyses of the ECMWF and the National Centers for Environmental Prediction (NCEP). The differences between the data from both reanalyses and global radiosonde observations is less than 2 K for most of the stations. ECMWF represents T_m slightly better than NCEP [*Wang et al.*, 2005]. In contrast, the estimation of T_m from surface temperature observations using the vertical temperature lapse rate given by *Bevis et al.* [1992] underestimates T_m in the tropics and subtropics by up to 6 K and overestimates T_m in the mid and high latitudes by up to 5 K [*Wang et al.*, 2005]. In this study the conversion of the ZWD into PW was carried out with T_m data from the ECMWF.

[13] In contrast to the temperature, pressure data from global analyses do not fulfill the accuracy requirements of 1 hPa required in the modeling of the hydrostatic delay [*Hagemann et al.*, 2003]. The surface pressure shows significant differences of more than 3 hPa between surface observations and ECMWF values for most of the stations of the IGS network. Over Antarctica large season-dependent differences of 2 to 6 hPa occur between the observations of automatic weather stations and the NCEP analysis [*Cullather et al.*, 1997]. Hence, surface pressure observations have to be applied instead of using data from numerical weather prediction (NWP) models.

[14] Today about 70 IGS stations are equipped with pressure sensors. However, only 17 of these stations can provide continuous pressure measurements for at least 6 years. Therefore, pressure observations from the large database of the World Meteorological Organization (WMO) comprising more than 14,000 stations worldwide were used. The maximum distance and the maximum height difference between the GPS and the WMO stations were restricted to 50 km and 500 m, respectively. The pressure observations from the WMO were available as daily mean values. A comparison of the daily mean pressure values from the IGS sensors and the neighboring WMO stations in Figure 1a reveals a bias of less than 1 hPa for more than 90% of the stations. For most of the stations the standard deviation between both observations is less than 2 hPa. However, some stations show significant differences between the IGS and the WMO pressure observations with a standard deviation of more than 4 hPa (Figure 1b). Most probably a drift in the IGS pressure sensor is the main reason for these large discrepancies. Figure 1c shows the example of the station Brussels, Belgium, where these drifts can reach up to 100 hPa/a. For pressure sensors from WMO stations no drift was detected. The results of *Hagemann et al.* [2003] showing that pressure observations from neighboring WMO stations very well represent the pressure at the GPS stations can be confirmed. WMO pressure time series are also preferable to the IGS pressure series regarding the length of their observation record, their continuity and their homogeneity. Pressure observations from the WMO stations were converted to the GPS antenna height using the hypsometric equation [*Stull*, 1995],

$$P_{GPS} = P_S \cdot e^{\frac{-g\cdot\Delta H}{R_d T}}, \tag{6}$$

with

P_{GPS} air pressure at GPS antenna height (hPa);
P_S air pressure at the height of the pressure sensor (hPa);
$\Delta H = H_{GPS} - H_S$ height difference (m);
g gravity acceleration (m $\cdot$ s^{-2});
$R_d = 287{,}053$ (JK^{-1} $\cdot$ kg^{-1}) gas constant of dry air;
T actual mean temperature of the layer between the GPS antenna and the meteorological sensor (K).

[15] For the PW estimation daily mean ZTDs were calculated to apply the daily mean pressure data. As this

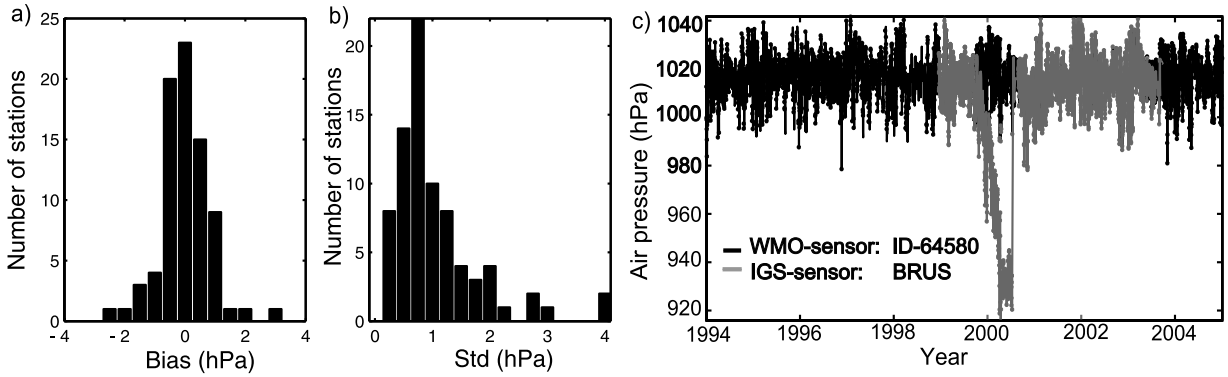

Figure 1. Comparison of the air pressure observations from neighboring IGS and WMO stations. (a) Histogram of the bias in the pressure, (b) histogram of the standard deviation of the pressure differences, and (c) comparison of the pressure time series from the WMO sensor (black) and the IGS sensor (gray) at the station Brussels (BRUS), Belgium.

paper concentrates on the annual and interannual changes in the PW the approach of using daily pressure observations instead of 3-hourly surface synoptic observations is passable. Before further interpretation a 3-sigma outlier check was carried out.

2.2. PW Results

[16] Precipitable water time series were derived for 141 stations using the WMO pressure observations. However, many PW time series do not cover the full period from 1994 to 2004 (Figure 2). For further analysis 62 stations covering a period of at least 7 years with data gaps smaller than 3 months were selected as a compromise between the time series length and the number of available stations.

[17] The consistency of the derived PW time series was evaluated using GPS/GPS colocations (Table 1). The standard deviation of the differences in the PW results at three colocated GPS sites is very small and ranges between 0.4 and 0.7 mm. For six GPS/GPS colocations without available pressure observations the zenith total delay was validated by *Steigenberger et al.* [2007]. The differences in the ZTD show standard deviations between 2.5 and 5.4 mm corresponding to 0.4 and 0.9 mm in PW. The reprocessing improved the precision of the tropospheric delay estimates by 20% compared to the IGS combined solution. This improvement is related to the application of advanced models in the reprocessing [*Steigenberger et al.*, 2007].

[18] One method of investigating the accuracy of the obtained results consists in comparing the tropospheric parameters from GPS and VLBI at colocated sites. A comparison of the ZWD parameters from the reprocessing with the ZWD estimates from VLBI using the same analysis strategy for both techniques was carried out by *Steigenberger et al.* [2007] at 27 colocated GPS/VLBI stations. For most of the stations the bias in the ZWD estimates between both techniques ranges from −5 to 9

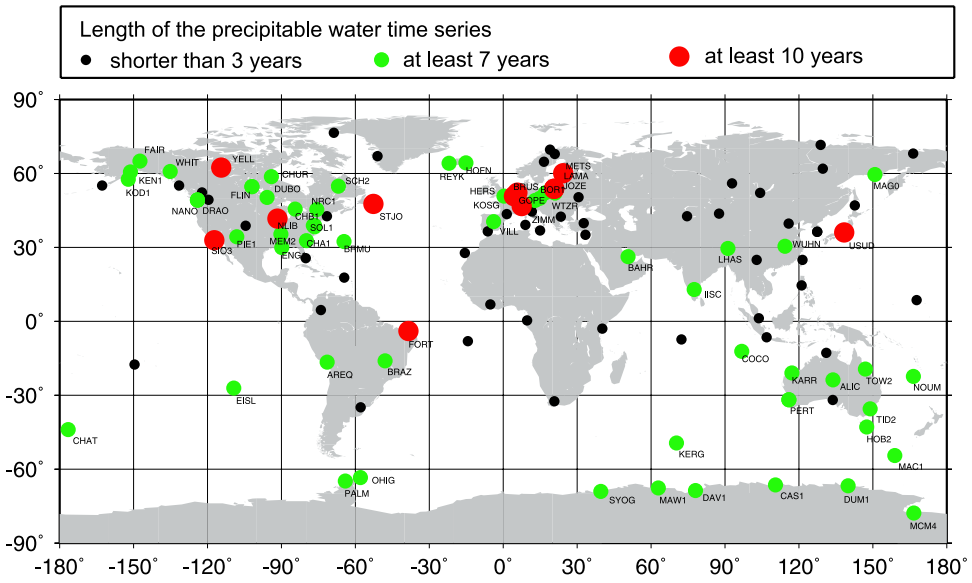

Figure 2. Length of the PW time series for all stations.

Table 1. Comparison of Daily Precipitable Water Values at GPS/GPS Colocations[a]

Station 1	Station 2	Number of Days With Common GPS Data	r	Bias (mm)	SD (mm)
WTZR	WETT	262	0.99	+0.02	0.38
TROM	TRO1	516	0.99	+0.03	0.70
YAKZ	YAKT	116	0.99	−0.01	0.39

[a]The r correlation coefficient, bias, and SD standard deviation of the PW differences.

mm and the RMS of the ZWD differences from 4 to 10 mm corresponding to an RMS in the PW of 0.7 to 1.7 mm. There are few stations showing larger differences between the ZWD values from both techniques. These stations are characterized by large height differences between the GPS and the VLBI antennas. In these cases the atmospheric water vapor located between the stations could have a remarkable impact on the ZWD bias. The water vapor in the atmospheric layer between the colocated stations was not considered in the ZWD comparison as the vertical distribution of the water vapor was unknown [*Steigenberger et al.*, 2007]. The accuracy of the PW estimates resulting from the error propagation of equations (1) and (4) mainly depends on the accuracy of the ZTD estimates, the pressure and the mean atmospheric temperature [*Bevis et al.*, 1994]. The mean temperature of the atmosphere T_m from ECMWF, which was used in this study, has an accuracy of better than 2 K [*Wang et al.*, 2005] As shown by *Hagemann et al.* [2003] and *Wang et al.* [2007] pressure observations from stations of the WMO in the surrounding of the GPS stations have an accuracy of better than 2 hPa. On the basis of the accuracy of the ZTD parameters of 4 to 10 mm and considering the mentioned uncertainties in the pressure and temperature the RMS of the PW estimates should be in the range of 1.1 to 1.9 mm. The accuracy obtained for the GPS PW is consistent with RMS errors of 1 to 3 mm from previous studies [e.g., *Bengtsson*, 2003; *Li et al.*, 2003; *Liou et al.*, 2000; *Vey et al.*, 2004; *Hagemann et al.*, 2003; *Gendt et al.*, 2004; *Deblonde et al.*, 2005; *Wang et al.*, 2007].

3. Analysis of the Homogeneity

[19] Homogeneous PW time series are prerequisite for the utilization of these time series for climatological investigations. The combined tropospheric parameters from the IGS solutions, which are provided beginning from 1997 until 2006, show inconsistencies of several millimeters due to changes in the used reference frame, the applied models and processing strategies [*Steigenberger et al.*, 2007]. Such processing-related inhomogeneities can be excluded for the reprocessing, as a consistent processing strategy was applied for the whole period from 1994 to 2004. However, changes in the hardware or in the software settings of the GPS station can significantly affect the GPS parameter estimation. Especially changes of the radome configuration can cause remarkable jumps in the PW time series. *Gardinarsky et al.* [2002] compared PW time series from GPS and radiosonde observations and found that the installation of a radome on top of a GPS antenna can cause significant jumps of 0.4 to 1.3 mm in the GPS-derived PW time series. These jumps are in the order of the expected climate-related changes in the precipitable water. Therefore,

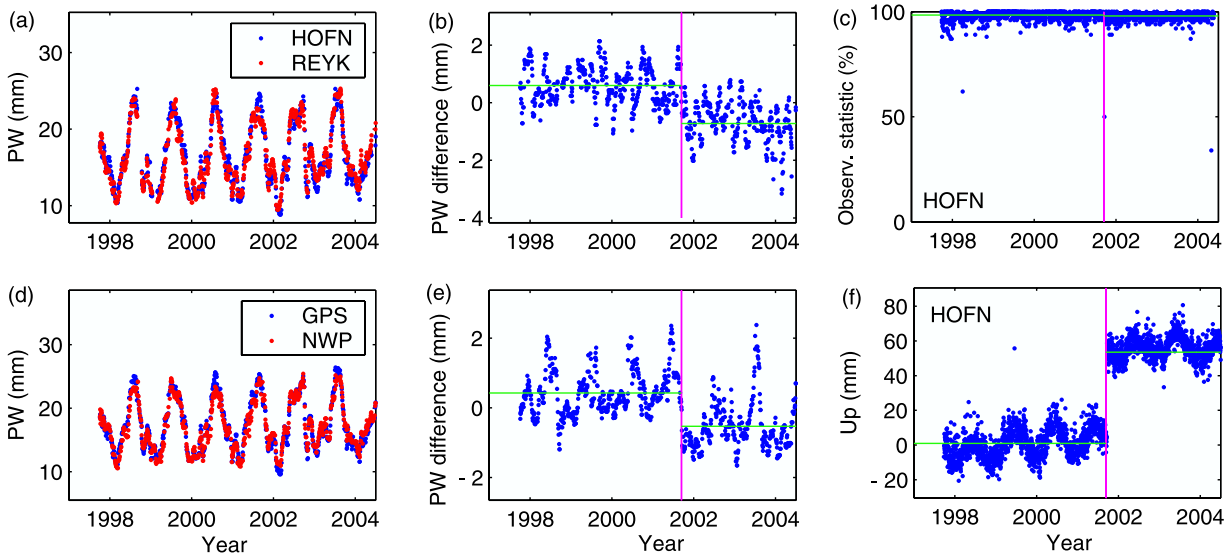

Figure 3. Influence of the installation of a radome on the PW estimates. (a) Comparison of the PW time series of the neighboring stations Hoefn (HOFN) and Reykjavik (REYK), Iceland, (b) time series of PW differences (HOFN-REYK), (c) observation statistics, (d) comparison of the PW time series from GPS and NCEP at HOFN, (e) time series of PW differences (GPS-NCEP), and (f) residuals in station height at HOFN. The installation of a radome and an antenna change in September 2001 causes a jump in the PW time series of the station HOFN of −1.3 mm.

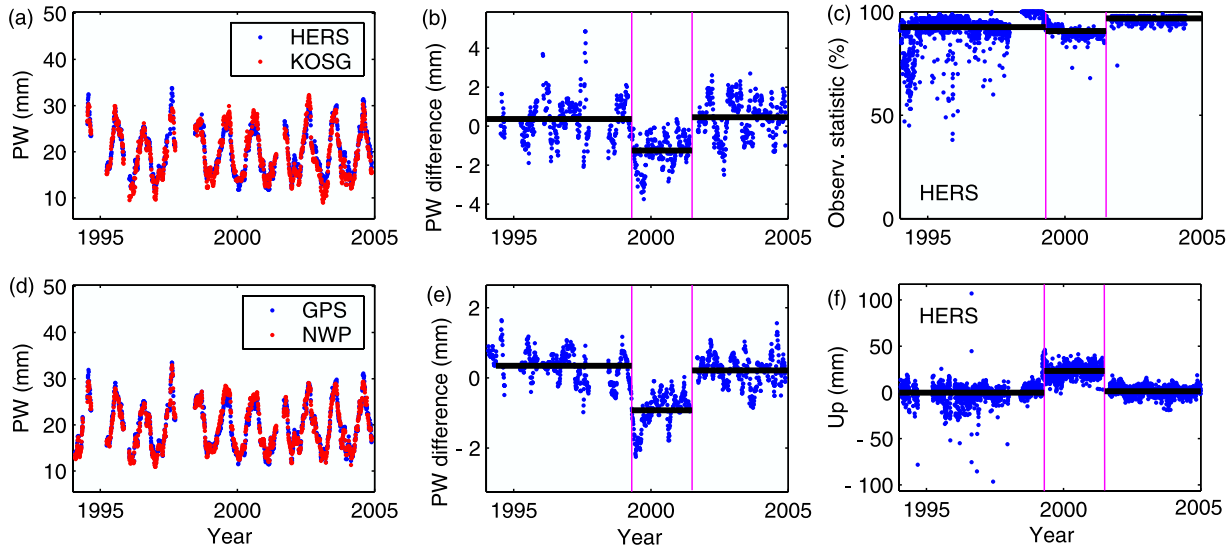

Figure 4. Influence of changes in the number of observations on the PW estimates. The lower PW values at station Hersmonceux (HERS), England, between March 1999 and June 2001 are related to a decrease in the number of observations recorded. As reference, station Kootwijk (KOSG) was used. For an explanation of plots, see Figure 3.

a detailed investigation of the homogeneity of the PW time series is very important.

3.1. Effects of Antenna and Radome Changes

[20] As visible in Figure 3a, the PW time series show strong seasonal signals of several centimeters. In contrast, inhomogeneities in the PW time series are in the millimeter range. Theoretically, climate signals and the effect of inhomogeneities could be separated by differencing the PW estimates at colocated stations. The climate signal affecting both stations in the same way would be canceled out and possible inhomogeneities would be visible. However, the periods of common data at most of the colocated GPS sites cover only some months. Observations from colocated VLBI stations cover longer periods, but they contain large data gaps. We therefore used the data of neighboring GPS stations with similar water vapor signals or data of the NWP model from NCEP. The differences calculated from these data have the disadvantage that they include, besides possible inhomogeneities, also spatial variations in the water vapor or uncertainties in the modeled PW.

[21] Figure 3a shows the PW time series of the stations Hoefn and Reykjavik in Iceland. The PW difference of both stations reveals a significant jump in September 2001 (Figure 3b). This jump is also visible in the comparison of the GPS-derived PW values at the station Hoefn with the PW data from NCEP (Figure 3e) as well as in the residuals of the height component of Hoefn (Figure 3f). The reason for the observed jump of 1.3 mm in the PW differences can be found in the mounting of a radome and an antenna change in September 2001. Other stations with PW time series influenced by jumps related to radome and/or antenna changes are presented in Figure 8.

3.2. Effects of Changes in the Observation Statistics

[22] Other jumps in the PW time series can be related to changes in the observation statistics, the ratio of all theoretically possible observations to the effectively recorded observations. In the example of the station Hersmonceux, England, in Figures 4a–4c the decrease in the observation statistics from 98% to below 90% causes smaller PW values on the order of 1.4 mm. This jump is visible in the PW difference of the stations Hersmonceux and Kootwijk, in the difference of the GPS- and NCEP-derived PW as well as in the residuals of the station height of Hersmonceux (Figures 4b, 4e and 4f). The parameters of the station height and the ZTD are strongly correlated depending on the observation geometry. A decrease in the number of observations influences the observation geometry. Hence, it causes a change in PW estimates. These changes in PW estimates are also related to the mapping function.

[23] As seen in Figure 5, biased PW estimates can be attributed also to a very low number of observations. The strong decrease in the observation statistics of the station Lamkowko, Poland, is related to a gradual breakdown of the GPS receiver between April and October 2000 causing errors in the PW estimates of more than 2 mm. These values are not detected in the 3-sigma outlier check, as their discrepancies are in the range of the natural PW variability. Only the differencing of PW time series and the comparison with other parameters like coordinates or the observation statistics can detect this kind of erroneous PW values.

[24] Jumps in the observation statistics are often related to changes in the elevation cutoff angle mask set at the receiver. We repeated the GPS reprocessing for the year 2002 with a cutoff elevation angle of 15° instead of 3° in order to determine the influence of changes in the elevation cutoff angle mask on the PW estimates. Figure 6 shows large differences between the ZTD estimates from both analyses. For 46% of the stations the mean annual ZTD change due to the change in the elevation cut off angle is larger than 1 mm. 10% of the stations show a change in the ZTD of more than 3 mm, corresponding to a change in PW of 0.5 mm. Very large elevation-dependent errors of up

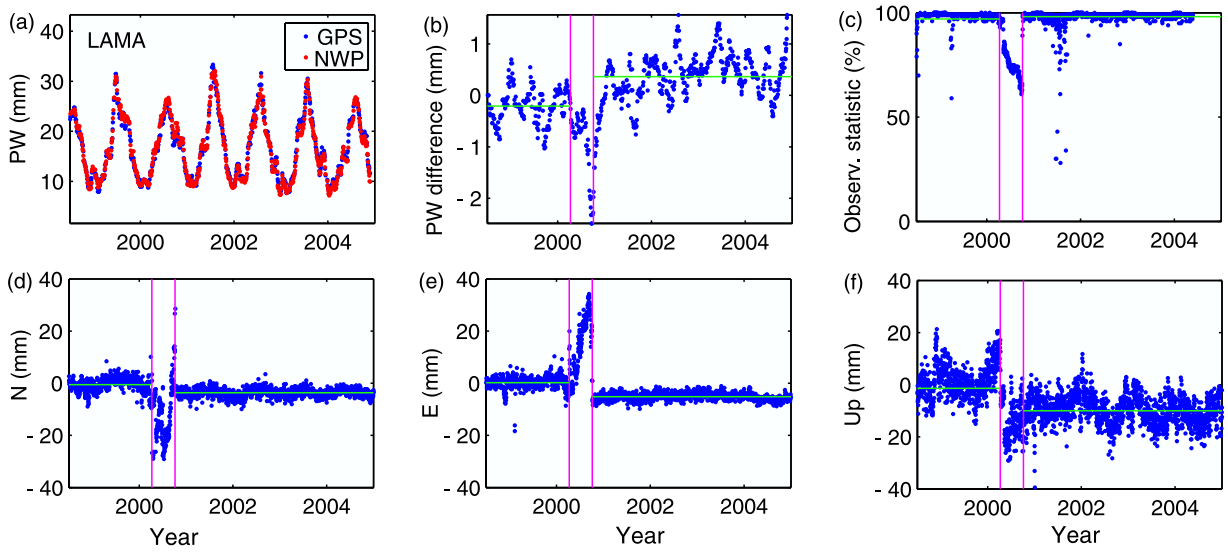

Figure 5. Influence of a strong decrease in the number of observations on the PW estimates, (a) PW at the station Lamkowko (LAMA), Poland. (b) The outliers in the PW difference time series (GPS–numerical weather prediction model (NWP)) as well as the (d–f) residuals in station height and position between April and October 2000 are characterized by (c) a strong decrease in the number of recorded GPS observations. This period corresponds to a slowly increasing failure of the GPS receiver. The subsequent replacement of the GPS antenna and receiver is the reason for the jump in the PW and the coordinate time series.

to 6 mm occur at stations with radomes. PW values from stations with radomes are more sensitive to changes in the cutoff elevation angle than stations without radomes. This behavior is caused by the effects radomes have on the antenna phase center variations which were not considered in the reprocessing.

[25] The introduction of absolute antenna phase center variations and the improvements made in the mapping function reduced the sensitivity of the estimated parameters to changes in the elevation cutoff angle mask [*Schmid et al.*, 2005; *Vey et al.*, 2006]. Despite the reduction of elevation-dependent errors its residual effect on the ZTD parameters cannot be neglected for the PW estimation (Figure 6).

[26] Besides the mentioned effects of antenna or radome changes as well as changes in the observation statistics no other effects could be detected affecting the homogeneity of the PW time series. Jumps in the coordinate time series related to earthquakes do not influence the ZTD time series confirming a correct separation of the ZTD and the height parameters.

3.3. Treatment of the Inhomogeneities

[27] A systematic investigation of all PW time series with the help of the IGS log files and the observation statistics shows that only one third of the PW time series can be assumed to be homogeneous (Figure 7). For an interpretation of the PW time series of all other stations a correction of the effects caused by changes in the GPS hardware or observation statistics is necessary. Most of the inhomogeneities are characterized by jumps in the PW time series. In these cases, an offset between the PW values before and after the occurrence of an event was estimated using the PW difference time series. As a premise for the offset estimation the parts of the difference time series before and after the event have to cover at least 1 year. The offset was estimated twice: First, for the PW difference time series from neighboring stations and, second, for the difference time series derived from GPS and NCEP PW. Both methods are independent from each other. The mean offsets derived from both methods are given in Figure 8. The offsets can reach values up to 1.3 mm. The accuracy of the offsets estimated from both methods ranges between 0.01 and

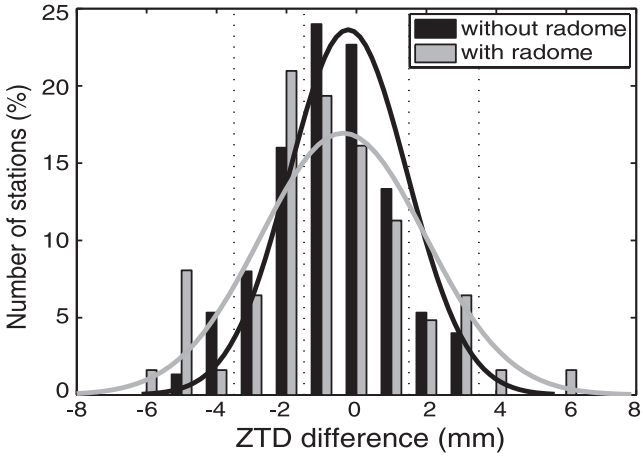

Figure 6. Influence of the cutoff elevation angle mask on the estimation of the zenith total delay. Mean differences in the ZTD parameters estimated for the year 2002 with an elevation mask of 3° and 15° for 72 stations with radome and 62 stations without radome.

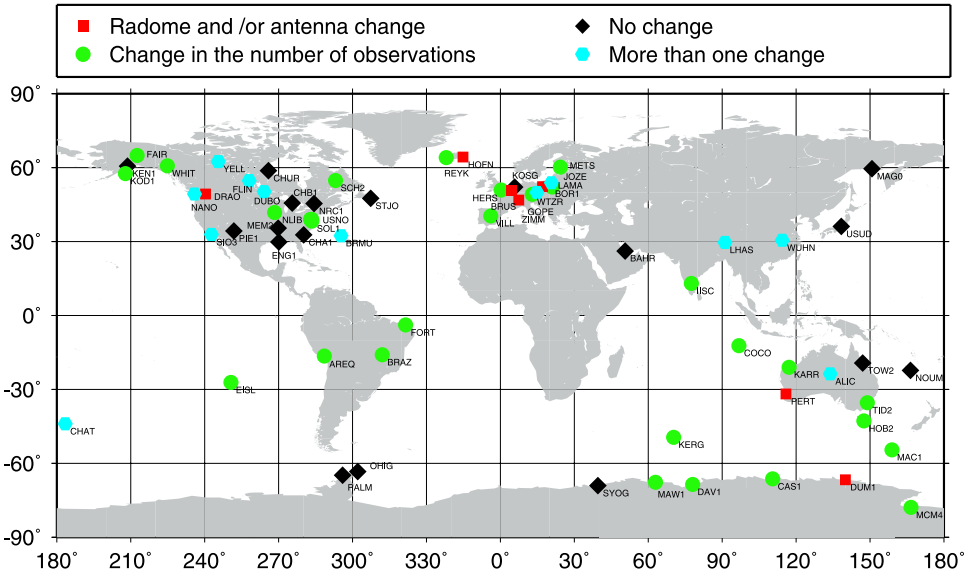

Figure 7. Overview of the homogeneity of the estimated PW time series.

0.4 mm. The best accuracy was obtained for PW time series differences with a small standard deviation covering long periods of time. The offset correction was applied to the part of the time series with the lower number of observations or to the part, where a radome was mounted on the GPS antenna. PW series with a slowly or irregularly changing observation statistics or an observation statistics of less than 75% were excluded from the subsequent analysis.

4. PW Anomalies

4.1. Time Series Analysis

[28] The main focus of the conducted times series analysis addresses the question: How has water vapor changed globally over the last decade? We therefore modeled the behavior of the PW not only as linear trend but considered also anomalies.

[29] First estimations of PW trends from geodetic observations were carried out for Scandinavia. Using data from GPS, radiosondes and water vapor radiometers in the time period from the end of 1993 until the end of 2000, *Gardinarsky et al.* [2002] estimated an increase in the integrated water vapor of 1 to 2 ± 1 mm/decade corresponding to 7–14% per decade of the mean PW. An extension of this study by 2 years shows similar results for the period from August 1993 until August 2002 [*Elgered et al.*, 2003]. Parameters of the tropospheric delay from the German station Wettzell estimated during a VLBI reprocessing analysis show an increase of 7 mm per decade [*Boehm et al.*, 2003]. This corresponds to an increase in the water vapor of about 1 mm per decade.

[30] In this paper, only stations of homogeneous time series with a length of at least 10 years were chosen for trend analyses. Time series were defined as homogeneous if they show no jumps or if the jumps could be corrected so that their effect on the trend estimation is less than 0.2 mm per decade. The results of the trend estimation from the eight stations fulfilling these criteria are presented in Table 2. In the time period from the begin of 1994 until the end of 2002 the stations in Europe show an increase in PW of 0.5 to 0.9 mm per decade. Within the confidence level these results confirm the trends published by *Gardinarsky et al.* [2002]. If the time period is extended until the end of 2004 the increase in the PW is much smaller and ranges between 0.2 and 0.3 mm per decade for the stations Brussels (BRUS) in Belgium, Kootwijk (KOSG) in the Netherlands and Metsahovi (METS) in Finland (Table 2).

[31] PW anomalies were defined as the deviations of the PW from a mean value. For this purpose a low-pass filter with a Finite Impulse Response (FIR) was applied to the time series. The advantage of FIR filters is that they are characterized by small transition zones and low ripples [*Kumar et al.*, 1992]. The applied FIR filter has a cutoff frequency of 0.8 cycles per year, a transition zone of 0.2 cycles per year and a ripple of 1%. All frequencies with a period higher than 1.4 years can pass almost completely whereas all frequencies with a period below 1.1 years are attenuated almost entirely. In this analysis only

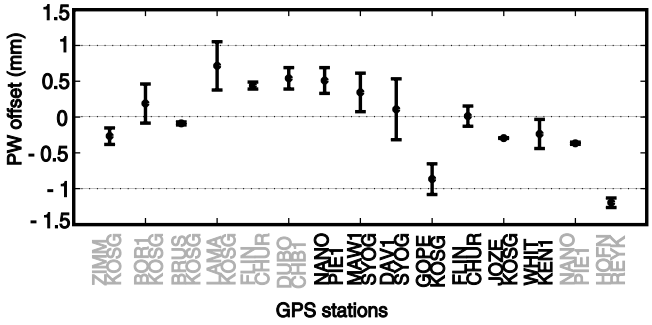

Figure 8. Estimated offsets in the PW time series caused by radome and/or antenna changes (gray) and changes in the number of observations (black).

Table 2. Estimated Trends in the PW[a]

Region	Station	$\overline{PW}$ (mm)	Trend 1994–2004 (%/decade)	Trend 1994–2004 (mm/decade)	Trend Difference of 10 and 11 Years (mm/decade)
Europe	BRUS	19.9	**0.85 ± 0.72**	0.17 ± **0.14**	−0.08
	KOSG	20.0	**1.39 ± 1.16**	0.28 ± **0.23**	+0.26
	METS	14.3	**1.41 ± 1.34**	0.20 ± **0.19**	+0.11
	ZIMM	17.0	−0.65 ± 1.13	−0.11 ± 0.19	+0.32
North America	NLIB	15.6	−0.07 ± 1.73	−0.01 ± 0.26	−0.24
	STJO	15.3	0.82 ± 0.85	0.13 ± 0.14	0.25
	YELL	7.2	−2.94 ± 4.04	−0.21 ± 0.29	0.16
East Asia	USUD	16.1	−0.43 ± 1.66	−0.07 ± 0.27	0.49

[a]Values marked in bold are significant at the 80% confidence level. $\overline{PW}$ represents the mean PW content over the time period from 1994 to 2004. The difference in the trend estimates is related to the time period from 1994 to 2003 and 1994 to 2004.

homogeneous time series or time series with an accuracy of the offset correction of better than 0.3 mm were included.

[32] Figure 9 represents the low-pass filtered time series. PW anomalies with ranges up to 2 mm are common for the stations on Iceland, in Europe, in Asia and in the region between 30°S and 60°S latitude. Most of the stations in North America show also PW anomalies with a range of 2 mm. An exception are the stations in the southern United States located near the Gulf of Mexico and the American Basin. The range of the PW anomalies in this region amounts to 4 mm which is twice as large as in the rest of North America (Figures 9a and 9b). Over Antarctica the interannual changes in the PW are smaller than 0.4 mm. The very small PW anomalies over Antarctica are related to the very low water vapor content in this region. In the tropics or in northern Australia, both regions with high water vapor content, the range of the PW anomalies can reach up to 10 mm (Figures 9f and 9g).

[33] The range of the PW anomalies strongly depends on the annual mean water vapor content. On the one hand, the water vapor content is influenced by the thermodynamical processes of condensation and evaporation; on the other hand, the water vapor content is linked to dynamical processes related to local and global circulations. *Zveryaev and Allan* [2005] investigated the influences of dynamical and thermodynamical processes on the temporal and spatial variations of the PW in the tropics in the period from 1979 to 2001 by using data from the ECMWF reanalysis. They found that changes in the water vapor content in the tropics are mainly influenced by large circulation pattern and are only to a small extent due to thermodynamical processes. In this study we investigate the influence of the thermodynam-

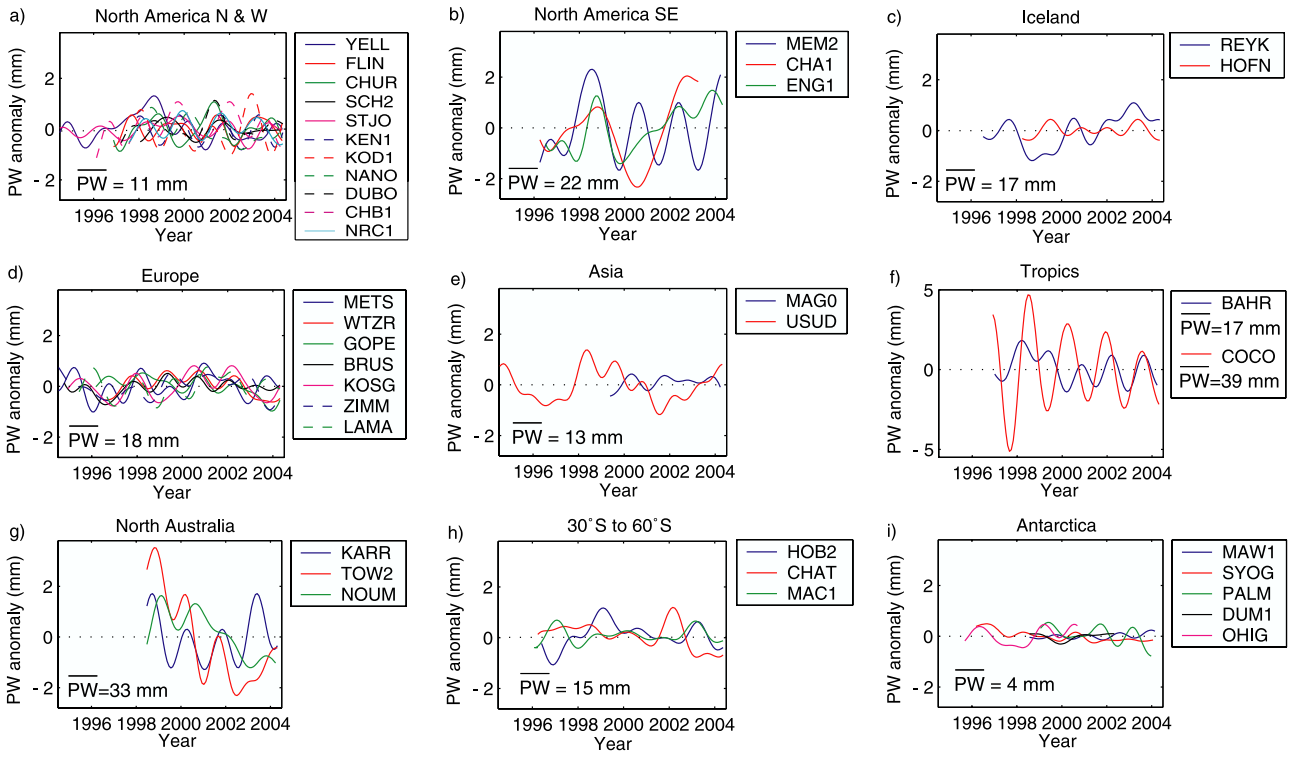

Figure 9. Anomalies of the precipitable water clustered regionally based on normalized data. $\overline{PW}$ represents the mean PW of all stations in the cluster. Figure 9f has a different scale.

ical and dynamical processes on the precipitable water globally. The knowledge about the reasons for PW variations is essential in the understanding of the feedback mechanism between temperature and water vapor.

4.2. Influence of the Temperature

[34] The Clausius-Clapeyron equation describes the temperature dependence of the saturation water vapor pressure e_s. From integration follows for e_s:

$$e_s = e_0 \cdot \exp\left[\frac{L}{R_v} \cdot \left(\frac{1}{T_0} - \frac{1}{T}\right)\right], \tag{7}$$

with

$e_0 = 0.611$ kPa — saturation partial water vapor pressure for $T_0 = 273$K

$R_v = 461.51$ (JK^{-1} kg^{-1}) — specific gas constant of water vapor

L — latent heat over ice surfaces $L = 2.83 \cdot 10^6$ (J kg^{-1}), over water surfaces $L = 2.50 \cdot 10^6$ (J kg^{-1}).

[35] If the atmosphere is heated by 1 K the air contains 7% more water assuming that the relative humidity stays constant. The partial water vapor pressure is related to the absolute humidity ρ_v by [*Stull*, 1995]

$$\rho_v = \frac{e_s}{R_v T}. \tag{8}$$

[36] Precipitable water is defined as the height of a water column produced by the condensation of all the absolute humidity contained in an air column of the height h (modified after *Bevis et al.* [1992]),

$$PW = \int_0^H \frac{\rho_v}{\rho_w} dh, \tag{9}$$

with ρ_w as the density of water.

[37] Using the equation of Clausius-Clapeyron and the equations (8) and (9), the PW of a saturated air column PW_s can be written as follows:

$$PW_s = \frac{1}{\rho_w} \int_0^H \frac{e_0 \cdot \exp\left[\frac{L}{R_v} \cdot \left(\frac{1}{T_0} - \frac{1}{T(h)}\right)\right]}{R_v T(h)} \cdot dh. \tag{10}$$

[38] We calculated PW_s using temperature data from the ECMWF. A comparison between the total precipitable water from GPS and PW_s is given in Figure 10. In the example of the station St. John's (STJO), Canada, the PW derived from GPS observations and the modeled PW agree very well. The seasonal as well as the interannual variations in PW can almost completely be reproduced by equation (10) (Figures 10a–10d). The increase and decrease in the water vapor of the station STJO can be explained entirely by changes in the air temperature.

[39] Figure 11 shows that for most of the stations in North America, Europe, Asia and stations in the high southern latitudes the water vapor content strongly depends on the atmospheric temperature. In regions with a high correlation between the modeled and the observed water vapor, thermodynamic processes are the reason for changes in the PW. For stations in lower latitudes the water vapor content is less dependent on temperature than for stations in high latitudes. In the tropics the temperature and the water vapor content even show a slightly negative correlation.

[40] In the example of the station Cocos Island (COCO) in the Indian Ocean represented in Figures 10e–10h the modeled PW_s is nearly constant over the year. The high water vapor content of this station from January to April corresponds to the monsoon period. The seasonal cycle in the water vapor content of the tropics is connected to atmospheric circulations causing the rain and dry seasons [*Weischet*, 1991]. The strong changes in the water vapor in the tropics which occur independently of temperature changes cause significant variations in the relative humidity. The assumption of a constant relative humidity being stated by some climate models is not fulfilled in the tropics [*Gaffen and Barnett*, 1992].

[41] For stations in northern Australia a part of the seasonal variations in the PW is attributed to seasonal temperature variations as they are shown as an example for station Karratha (KARR), in Figure 10k. However, the highest water vapor content in February and March is not related to a maximum in the temperature but is connected to the monsoon period in the southern autumn. In northern Australia the PW variations are caused by an overlap of dynamical processes related to humidity transports and thermodynamical processes.

[42] Interannual variations in the PW at the stations KARR and COCO represented in Figure 10h and 10l are negatively correlated with the modeled changes in the PW_s based on temperature anomalies. Additionally, in the tropics the amplitude of the observed PW anomalies is 3 to 4 times larger than the amplitude of the temperature induced PW_s anomalies. As seen at seasonal time scales, global circulation patterns are also the reason for water vapor anomalies at interannual time scales. The largest influence on the global circulation patterns at interannual time scales has the El Niño–Southern Oscillation (ENSO).

4.3. Influence of the Southern Oscillation

[43] The Southern Oscillation Index (SOI) quantifies the intensity of occurrence of the climate phenomena El Niño and La Niña. First studies of the SOI were carried out by, for example, *Trenberth* [1984]; *Ropelewski and Jones* [1987]. The SOI parameterizes the oscillation in the surface pressure between the southeastern tropical Pacific and the Australian-Indonesian regions. The SOI is defined as the ratio of the difference in the sea level pressure (SLP) of the stations Tahiti and Darwin, north Australia, and the mean standard deviation (MSD) of the air pressure differences of both stations,

$$SOI = \frac{SLP_{Tahiti} - SLP_{Darwin}}{MSD}. \tag{11}$$

[44] For a La Niña scenario the air pressure at Tahiti is higher than at Darwin, hence, the SOI is positive. In El Niño years the pressure situation in the tropical Pacific is inverted

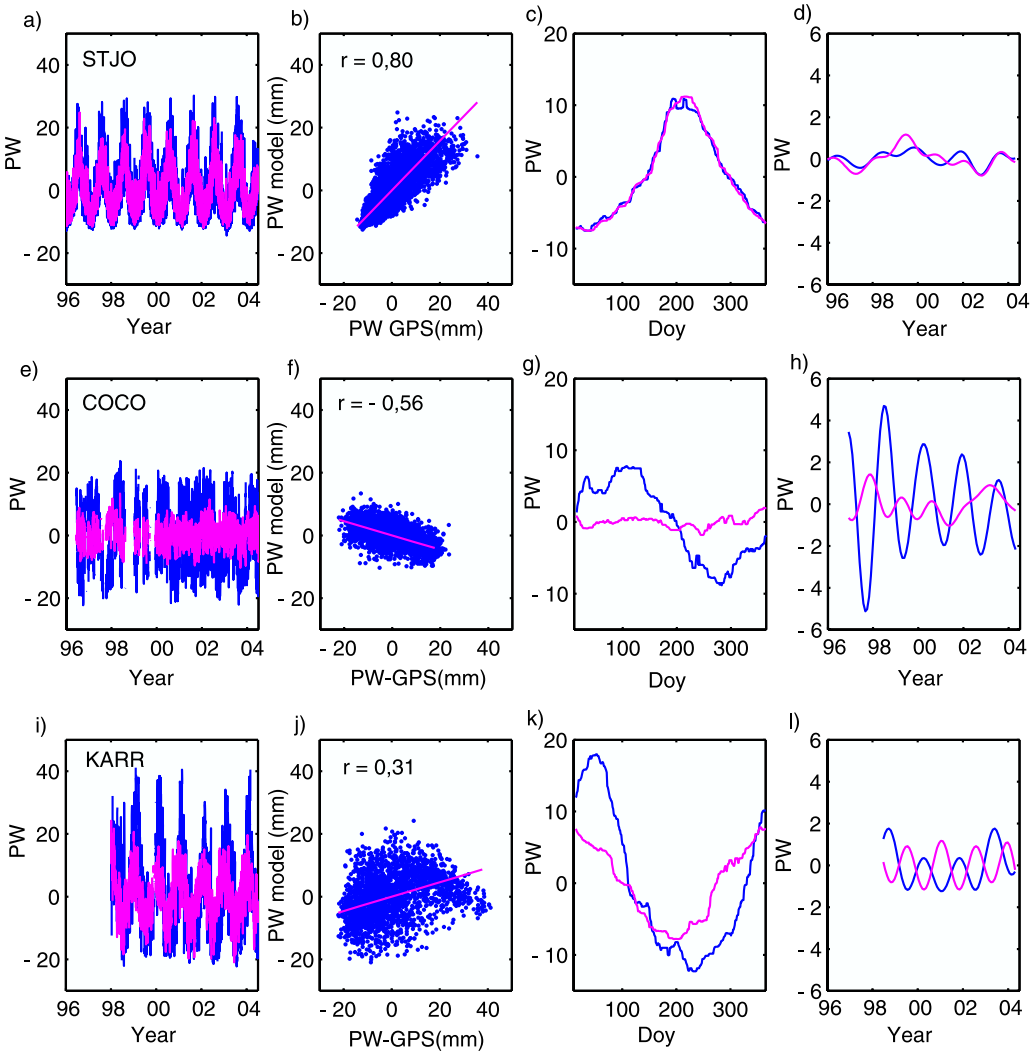

Figure 10. Comparison of the modeled PWs values based on the equation of Clausius-Clapeyron (magenta) and the GPS-derived PW values (blue) based on normalized data. (a) Comparison of daily values, (b) regression plot with the correlation coefficients *r*, (c) comparison of the seasonal signals, and (d) comparison of the PW anomalies for the station St. John's (STJO), Canada. Analog for the stations (e–h) Cocos Island (COCO) in the Indian Ocean and (i–l) Karratha (KARR), Australia.

and the SOI is negative. During the last 10 years the largest El Niño event occurred at the turn of the year 1997/1998 (Figure 12). The influence of El Niño on many distinct atmospheric and oceanic parameters was studied by numerous authors [e.g., *Neelin et al.*, 1998; *Philander*, 1990; *Trenberth and Caron*, 2000]. The largest impacts of ENSO were found in the tropical Pacific. However, ENSO also influences global climate processes [e.g., *Kiladis and Diaz*, 1989; *Yualeva and Wallace*, 1994; *Soden*, 2000; *Trenberth and Caron*, 2000; *Wagner et al.*, 2005; *Mokhov and Smirnov*, 2006]. These so-called teleconnections occur not only in the surroundings of the tropical Pacific like Australia and Asia, but also in far-off regions such as Europe or Antarctica [e.g., *Kidson and Renwick*, 2002; *Liu et al.*, 2002; *Mariotti et al.*, 2002]. The teleconnections influence a large number of different parameters, for example, ocean temperature, sea level height, air pressure, precipitation, cloud and sea ice coverage or radiation balance [e.g., *Ferraro et al.*, 1996; *Dai and Wigley*, 2000; *Zveryaev and Chu*, 2003; *Wu et al.*, 2003; *Guo and Bromwich*, 2004].

[45] Studies regarding the influence of ENSO on atmospheric water vapor cover mainly the tropics [e.g., *Ferraro et al.*, 1996; *Nanjundiah and Srinivasan*, 1999; *Soden*, 2000; *Foster et al.*, 2000; *Scaife et al.*, 2003; *Lu et al.*, 2004; *Wagner et al.*, 2005; *Zveryaev and Allan*, 2005]. Owing to the lack of radiosonde stations in the tropics most of these investigations use satellite microwave radiometer observations. However, at present the estimation of water vapor from satellite microwave radiometers is only reliable over the oceans [*Randel et al.*, 1996]. GPS observations on land are complementary to these satellite measurements. In a case study with two GPS stations in the tropical Pacific in

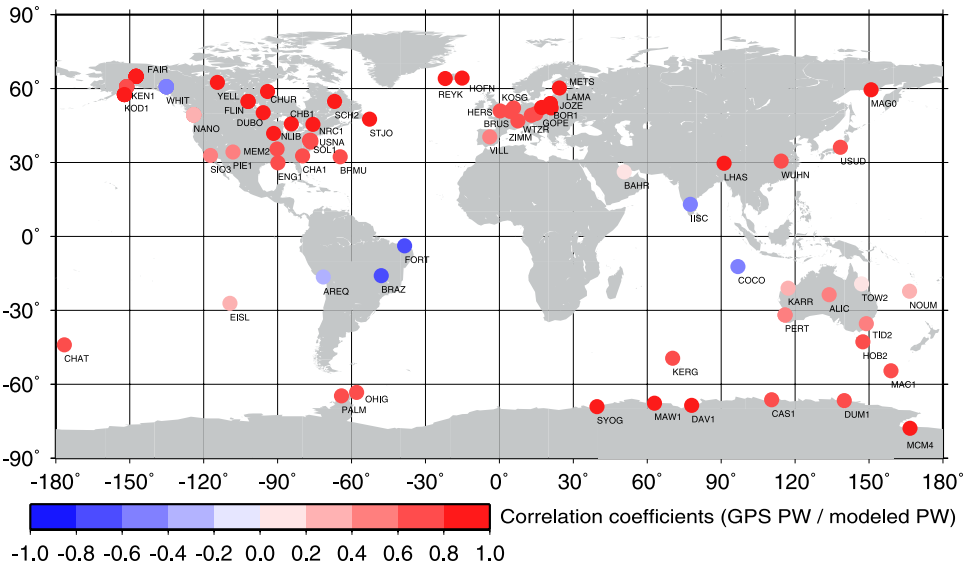

Figure 11. Correlation coefficients between the modeled PW values based on the equation of Clausius-Clapeyron and the GPS-derived PW.

the time period from 1997 to 1998, *Foster et al.* [2000] demonstrate the impact of El Niño on PW.

[46] Besides the anomalies in the PW here we also examined the anomalies in the variability of the PW. The variability was defined as the standard deviation of the daily PW values during 1 month after having removed a seasonal and an interannual signal from the time series. For the estimation of the anomalies in the variability the same filter was applied as to the PW series itself. The anomalies in the variability are exemplarily shown for the station Hobart (HOB2), Australia, in Figure 12. In the year 1997 the GPS-derived PW shows a strong negative anomaly being related to a high-pressure area which is predominant under the influence of El Niño over the western Pacific. The observed low water vapor content corresponds to large droughts over Australia during this time [*Gao et al.*, 2004]. The anomalies of the PW variability is also smaller under the impact of El Niño than under La Niña conditions. The water vapor anomalies of the other Australian stations behave similar to the PW at the station Hobart. Table 3 shows that the PW anomalies as well as the anomalies of the PW variability are positively correlated with the SOI at the six stations investigated. However, for most of the stations there are only weak anomaly-SOI correlations. The strongest correlations with 0.7 were found for the station TOW2. For this station which is directly located at the coast of the Pacific Ocean an influence of El Niño on the PW can be stated. With the exception of TOW2 the time series are too short to make definitive conclusions at this time. One interesting point to note is that the anomalies of the variability are generally higher correlated with SOI than the PW anomalies itself especially at station KARR.

5. Conclusions

[47] The installation or the change of radomes and GPS antennas significantly influences the PW results. Moreover, changes in the number of observations have also an impact on the PW estimates. These changes are often due to elevation cutoff angle changes. Modifications of the elevation cutoff angle from 3° to 15° can cause PW differences of up to 0.75 mm. For stations with radomes these differences can even reach up to 1 mm in PW.

[48] The main reasons for the sensitivity of the PW estimates to the elevation cutoff angle are uncertainties in the models of the antenna phase center variation and the mapping function. By the use of a mapping function based on a numerical weather prediction model and the application of an absolute antenna phase center model the dependence of the estimated parameters on the elevation cutoff angle was reduced compared to the standard IGS analysis. Nevertheless, there are residual uncertainties in the models which cannot be neglected when using PW time series for climatological studies. The consideration of radomes in the modeling of antenna phase center could further reduce the sensitivity of the PW estimates to elevation cutoff angle changes. GPS-derived PW time series have to be well-investigated for their homogeneity and detected jumps need to be corrected before the time series can be used to study

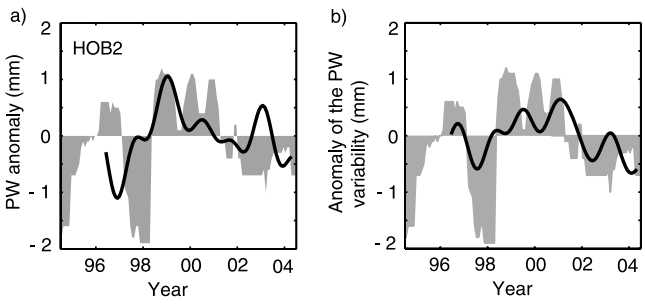

Figure 12. Comparison of the estimated anomalies (black) with the SOI (gray) at station Hobart (HOB2), Tasmania. (a) PW anomalies and (b) anomalies of the PW variability.

Table 3. Correlation Coefficient *r* of the Estimated Anomalies and the SOI Over Australia[a]

Station	*r* (SOI/PW Anomaly)	*r* (SOI/Anomaly of the Variability)
KARR	0.08 ± 0.29	0.72 ± 0.19
ALIC	0.37 ± 0.30	0.41 ± 0.30
TOW2	0.74 ± 0.17	0.76 ± 0.23
PERT	0.23 ± 0.27	0.40 ± 0.28
TID2	0.26 ± 0.25	0.53 ± 0.24
HOB2	0.26 ± 0.20	0.58 ± 0.22

[a]For most of the stations, *r* exceeds the 95% confidence level.

long-term changes in PW. Complete log files of all hardware and software changes are very useful for this check.

[49] For the investigation of interannual changes in PW the application of a low-pass filter has been preferred in comparison to the linear trend model, as the derived PW anomalies show a nonlinear behavior within the investigated timeframe. The range of the PW anomalies is smaller than 2 mm for most of the stations at high and mid latitudes. The PW anomalies in these regions are mainly caused by interannual variations in the atmospheric temperature. Larger PW anomalies with a range of up to 6 mm occur in the southeastern United States and northern Australia. In the tropics, PW anomalies with a range of up to 10 mm were detected. The PW anomalies of the station TOW2 confirm the correlation of the PW with the El Niño Southern Oscillation as presented by *Foster et al.* [2000]. Over Australia the El Niño periods are characterized by negative anomalies in the PW variability. The anomalies in the PW variability are stronger correlated with the Southern Oscillation than the PW anomalies itself. Owing to the significant interannual variations in the PW the GPS-derived time series at present are too short to draw conclusions on possible long-term trends in the PW.

[50] **Acknowledgments.** The investigations presented here were supported by the German Research Foundation (DFG). We gratefully acknowledge the constructive comments of the reviewers. Sincere thanks go to Johannes Böhm, for making the data of the height of the 200-hPa surface and the mean atmospheric temperature of the ECMWF available to us. We also thank NCEP for providing model data of precipitable water on its website. One of the authors (S. Vey) was partly supported by the "Studienstiftung des deutschen Volkes," which is gratefully acknowledged.

References

Bengtsson, L. U. A. (2003), The use of GPS measurements for water vapor determination, *Bull. Am. Meteorol. Soc.*, *67*, doi:10.1175/BAMS-84-9-1249.

Beutler, G, M. Rothacher, S. Schaer, T. A. Springer, J. Kouba, and R. E. Neilan (1999), The International GPS Service (IGS): An interdisciplinary service in support of Earth sciences, *Adv. Space Res.*, *23*(4), 631–635.

Bevis, M., S. Businger, T. A. Herring, A. Rocken, C. R. Anthes, and R. H. Ware (1992), GPS meteorology: Remote sensing of the atmospheric water vapor using the Global Positioning System, *J. Geophys. Res.*, *97*(D14), 15,787–15,801.

Bevis, M., S. Businger, S. Chiswell, T. A. Herring, R. A. Anthes, C. Rocken, and R. H. Ware (1994), GPS meteorology: Mapping zenith wet delays onto precipitable water, *J. Appl. Meteorol.*, *33*(3), 379–386.

Bock, O., C. Keil, E. Richard, C. Flamant, and M. N. Bouin (2005), Validation of precipitable water from ECMWF model analysis with GPS and radiosonde data during the MAP SOP, *Q. J. R. Meteorol. Soc.*, *131*(612), 3013–3036.

Bock, O., F. Guichard, S. Janicot, J. P. Lafore, M.-N. Bouin, and B. Sultan (2007), Multiscale analysis of precipitable water vapor over Africa from GPS data and ECMWF analyses, *Geophys. Res. Lett.*, *34*, L09705, doi:10.1029/2006GL028039.

Boehm, J., H. Schuh, V. Tesmer, and H. Schmitz-Hübsch (2003), Determination of tropospheric parameters by VLBI as a contribution to climatological studies, *Z. Vermessung Geoinf.*, *91*, 21–28.

Cullather, R. I., D. H. Bromwhich, and R. W. Grumbine (1997), Validation of operational numerical analyses in Antarctic latitudes, *J. Geophys. Res.*, *102*(D12), 13,761–13,784, doi:10.1029/96JD03328.

Dach, R., U. Hugentobler, P. Fridez, and M. Meindl (Eds.) (2007), *Bernese GPS Software Version 5.0*, Astron. Inst., Univ. of Bern, Bern.

Dai, A., and T. M. L. Wigley (2000), Global patterns of ENSO-induced precipitation, *Geophys. Res. Lett.*, *27*(9), 1283–1286, doi:10.1029/1999GL011140.

Deblonde, G., S. Macpherson, Y. Mireault, and P. Héroux (2005), Evaluation of GPS precipitable water over Canada and the IGS Network, *J. Appl. Meteorol.*, *44*(1), 153–166, doi:10.1175/JAM-2201.1.

Duan, J., M. Bevis, P. Fang, Y. Bock, S. Chiswell, S. Businger, C. Rocken, F. Solheim, and T. van Hove (1996), GPS meteorology: Direct estimation of the value of precipitable water, *J. Appl. Meteorol.*, *35*(6), 830–838, doi:10.1175/1520-0450(1996)035<0830:GMDEOT>2.0.CO;2.

Elgered, G., B. Stoew, L. Gradinarsky, and H. Bouma (2003), Analysis of atmospheric parameters derived from ground-based GPS observations, in *Proceedings of the International Workshop on GPS Meteorology*, edited by R. A. E. A. Anthes, pp. 3–11, Jpn. Int. Sci. and Technol. Exchange Cent., Tsukuba, Japan.

Elliott, W. P., and D. J. Gaffen (1991), On the utility of radiosonde humidity archives for climate studies, *Bull. Am. Meteorol. Soc.*, *72*, 1507–1520.

Ferrare, R. A., S. H. Melfi, D. N. Whiteman, K. D. Evans, F. J. Schmidlin, and D. O. Starr (1995), A comparison of water vapor measurements made by Raman lidar and radiosondes, *J. Atmos. Oceanic Technol.*, *12*(6), 1177–1195.

Ferraro, R., F. Weng, N. Grody, and A. Baptist (1996), An eight-year (1987–1994) time series of rainfall, clouds, water vapor, snow cover, and sea ice derived from SSM/I measurements, *Bull. Am. Meteorol. Soc.*, *77*, 891–905.

Folland, C. K., T. R. Karl, J. R. Christy, R. A. Clarke, G. V. Gruza, J. Jouzel, M. E. Mann, J. Oerlemanns, M. J. Salinger, and S. W. Wang (2001), Observed climate variability and change, in *Climate Change 2001: The Scientific Basis*, pp. 99–181, Cambridge Univ. Press, New York.

Foster, J., M. Bevis, T. Schroeder, M. Merrifield, S. Businger, S. Dorn, S. Marcus, J. Dickey, and Y. Bar-Server (2000), El Niño, water vapor, and the Global Positioning System, *Geophys. Res. Lett.*, *27*(17), 2697–2700, doi:10.1029/2000GL011429.

Fritsche, M., R. Dietrich, C. Knöfel, A. Rülke, S. Vey, M. Rothacher, and P. Steigenberger (2005), Impact of higher-order ionospheric terms on GPS estimates, *Geophys. Res. Lett.*, *32*, L23311, doi:10.1029/2005GL024342.

Gaffen, D. J., and T. P. Barnett (1992), A comparison of observations and model simulations of tropospheric water vapor, *J. Geophys. Res.*, *97*(D3), 2775–2780.

Gao, B.-C., P. K. Chan, and R.-R. Li (2004), A global water vapor data set obtained by merging the SSMI and MODIS data, *Geophys. Res. Lett.*, *31*, L18103, doi:10.1029/2004GL020656.

Garand, L., C. Grassotti, J. Hallé, and G. L. Klein (1992), On the differences in radiosonde humidity—Reporting practices and their implications for numerical weather prediction and remote sensing, *Bull. Am. Meteorol. Soc.*, *73*, 1417–1423.

Gardinarsky, L. P., J. M. Johansson, H. R. Bouma, H. G. Scherneck, and G. Elgered (2002), Climate monitoring using GPS, *Phys. Chem. Earth*, *27*(4–5), 335–340, doi:10.1016/S1474–7065(02)00009-8.

Gendt, G. (1998), IGS combination of tropospheric estimates—Experience from a pilot experiment, in *Proceedings of the IGS Analysis Center Workshop*, edited by J. M. Dow et al., pp. 205–216, Eur. Space Agency, Darmstadt, Germany.

Gendt, G., G. Dick, C. Reigber, M. Tomassini, Y. Liu, and M. Ramatschi (2004), Near real time GPS water vapor monitoring for numerical weather prediction in Germany, *J. Meteorol. Soc. Jpn.*, *82*(1B), 361–380.

Guerova, G., J.-M. Bettems, E. Brockmann, and C. Matzler (2006), Assimilation of COST 716 near-real time GPS data in the nonhydrostatic limited area model used at MeteoSwiss, *Meteorol. Atmos. Phys.*, *91*(1–4), 149–164, doi:10.1007/s00703-005-0110-6.

Guo, Z., and D. H. Bromwich (2004), Modeled antarctic precipitation. Part II: ENSO modulation over West Antarctica, *J. Clim.*, *17*(3), 448–465, doi:10.1175/1520-0442(2004)017<0448:MAPPIE>2.0.CO;2.

Gutman, S. I., and S. G. Benjamin (2001), The role of ground-based GPS meteorological observations in numerical weather prediction, *GPS Solutions*, *4*(4), 16–24.

Hagemann, S., L. Bengtsson, and G. Gendt (2003), On the determination of atmospheric water vapor from GPS measurements, *J. Geophys. Res.*, *108*(D21), 4678, doi:10.1029/2002JD003235.

Hall, A., and S. Manabe (1999), The role of water vapor feedback in unperturbed climate variability and global warming, *J. Clim.*, *12*(8), 2327–2346, doi:10.1175/1520–0442(1999)012<2327:TROWVF>2.0.CO;2.

Held, I. M., and B. J. Soden (2000), Water vapor feedback and global warming, *Annu. Rev. Energy Environ.*, *25*, 441–475.

Kidson, J. W., and J. A. Renwick (2002), The Southern Hemisphere evolution of ENSO during 1981–99, *J. Clim.*, *15*(8), 847–863, doi:10.1175/1520–0442(2002)015<0847:TSHEOE>2.0.CO;2.

Kiladis, G. N., and H. F. Diaz (1989), Global climatic anomalies associated with extremes in the Southern Oscillation, *J. Clim.*, *2*(9), 1069–1090, doi:10.1175/1520–0442(1989)002<1069:GCAAWE>2.0.CO;2.

Kumar, B., R. S. C. Dutta, and H. Shah (1992), On the design of FIR digital differentiators, *IEEE Trans. Signal Process.*, *40*(9), 2334–2338, doi:10.1109/78.157235.

Li, Z., J.-P. Muller, and P. Cross (2003), Comparison of precipitable water vapor derived from radiosonde, GPS, and Moderate-Resolution Imaging Spectroradiometer measurements, *J. Geophys. Res.*, *108*(D20), 4651, doi:10.1029/2003JD003372.

Liou, Y. A., C. Y. Huang, and Y. T. Teng (2000), Precipitable water observed by ground-based GPS receivers and microwave radiometry, *Earth Planets Space*, *52*, 445–450.

Liu, J., X. Yuan, D. Rind, and D. G. Martinson (2002), Mechanism study of the ENSO and southern high latitude climate teleconnections, *Geophys. Res. Lett.*, *29*(14), 1679, doi:10.1029/2002GL015143.

Lu, R., B. Dong, R. D. Cess, and G. L. Potter (2004), The 1997/98 El Niño: A test for climate models, *Geophys. Res. Lett.*, *31*, L12216, doi:10.1029/2004GL019956.

Mariotti, A., N. Zeng, and K. M. Lau (2002), Euro-Mediterranean rainfall and ENSO—A seasonally varying relationship, *Geophys. Res. Lett.*, *29*(12), 1621, doi:10.1029/2001GL014248.

Miloshevich, L. M., H. Vömel, A. Paukkunen, A. J. Heymsfield, and S. J. Oltmans (2001), Characterization and correction of relative humidity measurements from Vaisala RS80-A radiosondes at cold temperatures, *J. Atmos. Oceanic Technol.*, *18*(2), 135–156, doi:10.1175/1520–0426(2001)018<0135:CACORH>2.0.CO;2.

Miloshevich, L. M., H. Vömel, D. N. Whiteman, B. M. Lesht, F. J. Schmidlin, and F. Russo (2006), Absolute accuracy of water vapor measurements from six operational radiosonde types launched during AWEX-G and implications for AIRS validation, *J. Geophys. Res.*, *111*, D09S10, doi:10.1029/2005JD006083.

Mokhov, I. I., and D. A. Smirnov (2006), El Niño–Southern Oscillation drives North Atlantic Oscillation as revealed with nonlinear techniques from climatic indices, *Geophys. Res. Lett.*, *33*, L03708, doi:10.1029/2005GL024557.

Nanjundiah, R. S., and J. Srinivasan (1999), Anomalies of precipitable water vapour and vertical stability during El Niño, *Geophys. Res. Lett.*, *26*(1), 95–98.

Neelin, D., D. Battisti, A. Hirst, F. F. Jin, Y. Wakata, T. Yamagata, and S. Zebiak (1998), ENSO theory, *J. Geophys. Res.*, *103*(C7), 14,262–14,290.

Niell, A. E. (2000), Improved atmospheric mapping functions for VLBI and GPS, *Earth Planets Space*, *52*, 699–702.

Philander, G. S. (1990), *El Niño, La Niña and the Southern Oscillation*, 289 pp., Elsevier, New York.

Philipona, R., B. Dürr, A. Ohmura, and C. Ruckstuhl (2005), Anthropogenic greenhouse forcing and strong water vapor feedback increase temperature in Europe, *Geophys. Res. Lett.*, *32*, L19809, doi:10.1029/2005GL023624.

Randel, D. L., T. H. Vonder Haar, M. A. Ringerud, G. L. Stephens, T. J. Greenwald, and C. L. Combs (1996), A new global water vapor dataset, *Bull. Am. Meteorol. Soc.*, *77*, 1233–1246.

Rocken, C., R. Ware, H. T. Van, F. Solheim, C. Alber, and J. Johnson (1993), Sensing atmospheric water vapor with the Global Positioning System, *Geophys. Res. Lett.*, *20*(23), 2631–2634.

Rocken, C., T. Van Hove, J. Johnson, F. Solheim, R. Ware, M. Bevis, S. Chiswell, and S. Businger (1995), GPS/STORM-GPS sensing of atmospheric water vapor for meteorology, *J. Atmos. Oceanic Technol.*, *12*(3), 468–478.

Ropelewski, C. F., and P. D. Jones (1987), An extension of the Tahiti-Darwin Southern Oscillation, *Mon. Weather Rev.*, *115*(9), 2161–2165, doi:10.1175/1520–0493(1987)115<2161:AEOTTS>2.0.CO;2.

Ross, R. J., and W. P. Elliott (1996), Tropospheric water vapor climatology and trends over North America: 1973–93, *J. Clim.*, *9*(12), 3561–3574, doi:10.1175/1520–0442(1996)009<3561:TWVCAT>2.0.CO;2.

Ross, R. J., and W. P. Elliott (2001), Radiosonde-based Northern Hemisphere tropospheric water vapor trends, *J. Clim.*, *14*(7), 1602–1612, doi:10.1175/1520–0442(2001)014<1602:RBNHTW>2.0.CO;2.

Saastamoinen, J. (1972), Atmospheric corrections for the troposphere and stratosphere in radio ranging of satellites, in *The Use of Artificial Satellites for Geodesy*, *Geophys. Monogr. Ser.*, vol. 15, edited by S. W. Henriksen et al., pp. 247–251, AGU, Washington, D. C.

Scaife, A. A., N. Butchart, D. R. Jackson, and R. Swinbank (2003), Can changes in ENSO activity help to explain increasing stratospheric water vapor?, *Geophys. Res. Lett.*, *30*(17), 1880, doi:10.1029/2003GL017591.

Schmid, R., M. Rothacher, D. Thaller, and P. Steigenberger (2005), Absolute phase center corrections of satellite and receiver antennas, *GPS Solutions*, *9*(4), 283–293, doi:10.1007/s10291-005-0134-x.

Schneider, E. K., B. P. Kirtman, and R. S. Lindzen (1999), Tropospheric water vapor and climate sensitivity, *J. Atmos. Sci.*, *56*(11), 1649–1658, doi:10.1175/1520–0469.

Soden, B. J. (2000), The sensitivity of the tropical hydrological cycle to ENSO, *J. Clim.*, *13*(3), 538–549, doi:10.1175/1520–0442(2000)013<0538:TSOTTH>2.0.CO;2.

Soden, B. J., and J. R. Lanzante (1996), An assessment of satellite and radiosonde climatologies of upper-tropospheric water vapor, *J. Clim.*, *9*(6), 1235–1250.

Soden, B. J., R. T. Wetherald, G. L. Stenchikov, and A. Robock (2002), Global cooling after the eruption of Mount Pinatubo: A test of climate feedback by water vapor, *Science*, *296*(5568), 727–730, doi:10.1126/science.296.5568.727.

Steigenberger, P., M. Rothacher, R. Dietrich, M. Fritsche, A. Rülke, and S. Vey (2006), Reprocessing of a global GPS network, *J. Geophys. Res.*, *111*, B05402, doi:10.1029/2005JB003747.

Steigenberger, P., V. Tesmer, M. Krügel, D. Thaller, R. Schmid, S. Vey, and M. Rothacher (2007), Comparisons of homogeneously reprocessed GPS and VLBI long time-series of troposphere zenith delays and gradients, *J. Geod.*, *81*(6–8), 503–514, doi:10.1007/s00190-006-0124-y.

Stull, R. B. (1995), *Meteorology for Scientists and Engineers—A Technical Companion Book*, West, Minneapolis, Minn.

Su, H., W. G. Read, J. H. Jiang, J. W. Waters, D. L. Wu, and E. J. Fetzer (2006), Enhanced positive water vapor feedback associated with tropical deep convection: New evidence from Aura MLS, *Geophys. Res. Lett.*, *33*, L05709, doi:10.1029/2005GL025505.

Tregoning, P., R. Boers, D. O'Brien, and M. Hendy (1998), Accuracy of absolute precipitable water vapor estimates from GPS observations, *J. Geophys. Res.*, *103*(D22), 28,701–28,710, doi:10.1029/98JD02516.

Trenberth, K. E. (1984), Interannual variability of the Southern Hemisphere circulation: Representativeness of the year of the Global Weather Experiment, *Mon. Weather Rev.*, *112*(1), 108–123.

Trenberth, K. E., and J. M. Caron (2000), The Southern Oscillation revisted: Sea level pressures, surface temperatures, and precipitation, *J. Clim.*, *13*(24), 4358–4365, doi:10.1175/1520–0442(2000)013<4358:TSORSL>2.0.CO;2.

Vedel, H., X.-Y. Huang, J. Haase, M. Ge, and E. Calais (2004), Impact of GPS Zenith Tropospheric Delay data on precipitation forecasts in Mediterranean France and Spain, *Geophys. Res. Lett.*, *31*, L02102, doi:10.1029/2003GL017715.

Vey, S., R. Dietrich, K. P. Johnsen, J. Miao, and G. Heygster (2004), Comparison of tropospheric water vapour over Antarctica derived from AMSU-B data, ground-based GPS data and the NCEP/NCAR Reanalysis, *J. Meteorol. Soc. Jpn.*, *82*(1B), 259–267.

Vey, S., R. Dietrich, M. Fritsche, A. Rülke, M. Rothacher, and P. Steigenberger (2006), Influence of mapping function parameters on global GPS network analyses: Comparisons between NMF and IMF, *Geophys. Res. Lett.*, *33*, L01814, doi:10.1029/2005GL024361.

Wagner, T., S. Beirle, M. Grzegorski, S. Sanghavi, and U. Platt (2005), El Niño induced anomalies in global data sets of total colum precipitable water and cloud cover derived from GOME on ERS-2, *J. Geophys. Res.*, *110*, D15104, doi:10.1029/2005JD005972.

Wang, J., L. Zhang, and A. Dai (2005), Global estimates of water-vapor-weighted mean temperature of the atmosphere for GPS applications, *J. Geophys. Res.*, *110*, D21101, doi:10.1029/2005JD006215.

Wang, J., L. Zhang, A. Dai, T. Van Hove, and J. Van Baelen (2007), A near-global, 2-hourly data set of atmospheric precipitable water from ground-based GPS measurements, *J. Geophys. Res.*, *112*, D11107, doi:10.1029/2006JD007529.

Weischet, W. (1991), *Einführung in die Allgemeine Klimatologie*, Teubner, Stuttgart.

Wickert, J., G. Beyerle, R. König, S. Heise, L. Grunwaldt, G. Michalak, C. Reigber, and T. Schmidt (2005), GPS radio occultation with CHAMP and GRACE: A first look at a new and promising satellite configuration for global atmospheric sounding, *Ann. Geophys.*, *23*(3), 653–658.

Wu, R., Z. Z. Hu, and B. P. Kirtman (2003), Evolution of ENSO-related rainfall anomalies in east Asia, *J. Clim.*, *16*(22), 3742–3758, doi:10.1175/1520–0442(2003)016<3742:EOERAI>2.0.CO;2.

Yualeva, E., and J. M. Wallace (1994), The signature of ENSO in global temperature and precipitation fields derived from the microwave sounding unit, *J. Clim.*, *7*(11), 1719–1736, doi:10.1175/1520–0442(1994)007<1719:TSOEIG>2.0.CO;2.

Yunck, T. P., C. H. Liu, and R. Ware (2000), A history of GPS sounding, *Terr. Atmos. Oceanic Sci.*, *11*(1), 1–20.

Zhai, P., and R. E. Eskridge (1996), Analyses of inhomogeneities in radiosonde temperature and humidity time series, *J. Clim.*, *9*(4), 884–894, doi:10.1175/1520–0442(1996)009<0884:AOIIRT>2.0.CO;2.

Zveryaev, I. I., and R. P. Allan (2005), Water vapor variability in the tropics and its links to dynamics and precipitation, *J. Geophys. Res.*, *110*, D21112, doi:10.1029/2005JD006033.

Zveryaev, I. I., and P.-S. Chu (2003), Recent climate changes in precipitable water in the global tropics as revealed in National Centers for Environmental Prediction–National Center for Atmospheric Research reanalysis, *J. Geophys. Res.*, *108*(D10), 4311, doi:10.1029/2002JD002476.

R. Dietrich, M. Fritsche, A. Rülke, and S. Vey, Institut für Planetare Geodäsie, Technische Universität Dresden, D-01062 Dresden, Germany. (sibylle.vey@web.de)

M. Rothacher, Institut für Geodäsie und Photogrammetrie, Eidgenössische Technische Hochschule Zürich, ETH-Hönggerberg, Schafmattstraße 34, CH-8093 Zürich, Switzerland.

P. Steigenberger, Institut für Astronomische und Physikalische Geodäsie, Technische Universität München, D-80290 München, Germany.